CHAPTER 5

Real-time computer modeling in prevention of foot pressure ulcer using patient-specific finite element model and model order reduction techniques

S. Niroomandi[1], A. Perrier[1,2], M. Bucki[2], Yohan Payan[1]
[1]*Laboratoire TIMC-IMAG, CNRS & University Grenoble Alpes, France;*
[2]*TexiSense, Montceau-les-Mines, France*

Chapter Outline

1. Introduction

This chapter summarizes some technologies that could be used to help with prevention of diabetic foot pressure ulcer. The latest work from the authors is also presented. The first component is a fully wireless, customizable, and washable smart sock to monitor the pressure applied to the foot. The second component is a patient-specific finite element (FE) model of the foot including soft tissues and bony prominences, which is specifically built and used to compute the internal strains and stresses from the pressure data provided by the smart sock sensors. To simulate such complex model, the ArtiSynth platform (artisynth.org) was used. Although ArtiSynth is powerful in combining rigid bodies and soft tissues, simulation time is in the order of hours, which is not suitable for a monitoring device. To overcome this issue, we could use a reduced order model (ROM) to decrease

Innovations and Emerging Technologies in Wound Care. https://doi.org/10.1016/B978-0-12-815028-3.00005-5

computation time to less than a second and thus make the simulations run in real time. In the following sections, foot pressure ulcer and associated complications are briefly reviewed while the smart diabetic socks are described. Then a patient-specific foot model from the authors is presented. Afterward, main ideas of model order reduction techniques that are used, namely proper orthogonal decomposition (POD) and POD with interpolation (PODI), are reviewed. After the ROM is constructed, a displacement field for evaluation points was simulated in a time frame of about 0.1s. Despite such short computation time, the results of the ROM show good accuracy in comparison to the full ArtiSynth solution and the maximum relative error norm was 4.6%, which seems acceptable from a clinical point of view. This technique could equally be extended to use an online version of the foot model by applying pressure values measured by the smart sock.

2. Foot ulcer and smart diabetic socks

Foot ulcers are mostly the consequence of a trauma or excessive pressures associated to diabetes and resulting from repetitive high stresses and strains, ill-fitting footwear, or sometimes an external object inside the shoe. Diabetic peripheral neuropathy and angiopathy are chronic complications of diabetes affecting the lower limbs. When both complications are associated to an external trivial trauma, they determine the progression of the pathology from a nonulcerated condition of a foot at risk to an acute syndrome characterized by the classic diabetic foot ulcer, followed by a chronic condition in the postulcerative phase, which can lead to amputation [1]. Healthy individuals with undamaged somatosensory function would experience pain and avoid the offending pressures if such external trauma occurred. On the contrary, in a person who suffers from diabetic neuropathy there is no warning of excessive pressure or tissue damage, which could lead to skin breakdown or ulceration. Previous studies suggested that an efficient care could reduce foot ulcer [2]. This monitoring strategy is largely based on renewed vigilance of the diabetic patient, which mainly consists in making a daily inspection of his/her feet. Unfortunately, studies show that patient vigilance decreases over time and complications which appear after some time are directly correlated with the increasing lack of vigilance. In the case of diabetic patients, it is precisely when the first foot ulcers appear that serious complications begin. This is mainly due to recurrent disease in the diabetic angiopathy, which severely limits the healing process. It becomes therefore essential to propose new technologies and services dedicated to the monitoring and assistance of the diabetic patient to help maintain his/her alertness and by extension his/her autonomy in society. The external trauma that causes tissue breakdown could be intrinsic, such as repetitive stresses from high pressure and/or callus, or extrinsic, such as from ill-fitting footwear rubbing on the skin or an object inside the shoe. It hence appears very suitable to be able (1) to monitor the external pressure applied all around the foot and (2) if possible, to estimate the corresponding internal stresses and strains.

To monitor the external pressures, a fully wireless customizable and washable smart sock was designed in a collaboration between two research laboratories (TIMC-IMAG and AGIM), three companies (TexiSense, IDS, and IFTH), and a clinical center (Center de l'Arche) in France [3].This smart sock is made of three main components: a 100% textile sock that collects the foot external pressures, a central unit, and an external device that receives the wireless information sent by the central unit and estimates the risks for pressure ulcer. A schematic of this system and details of the sock and its embedded sensors are shown in Figs. 5.1 and 5.2, respectively.

It is now well established that measuring pressures at the skin surface is not sufficient to prevent the most dangerous foot ulcers that start in deep tissues and progress outward rapidly, causing substantial subcutaneous damage underneath intact skin [22,4]. Indeed, such surface measurements are not sufficient to predict ulcer formation caused by internal tissue loading [5,6]. For example, a very similar pressure distribution could be observed under the heel of a thin person with blunt calcaneus bone and of a heavy diabetic person with sharp calcaneus bone, whereas in that case, the diabetic person has obviously much higher risks for foot pressure ulcers. The likelihood of a pressure ulcer forming is

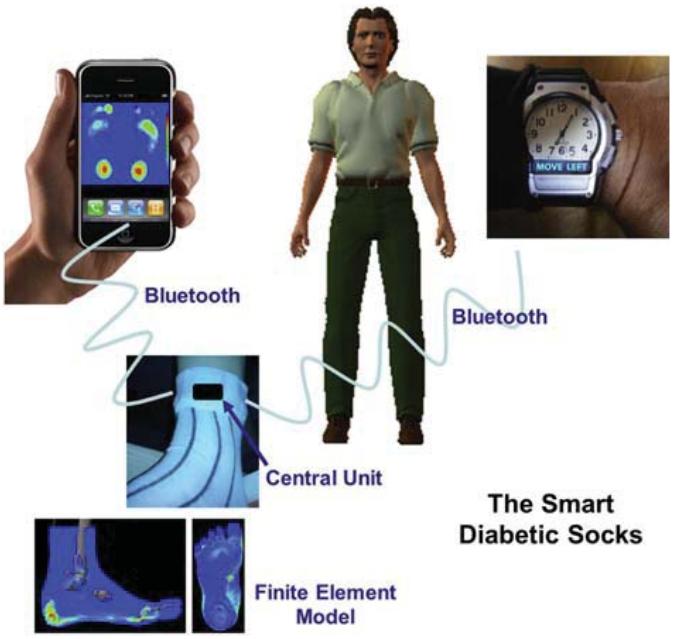

Figure 5.1

This smart sock is made of three main components: a 100% textile sock that collects the foot external pressures, a central unit, and an external device that receives the wireless information sent by the central unit and estimates the risks for pressure ulcer. *From Perrier A, Vuillerme N, Luboz V, Bucki M, Cannard F, Diot B, Colin D, Rin D, Bourg J-P, Payan Y. Smart Diabetic Socks: embedded device for diabetic foot prevention. IRBM April 2014; 35:72–6.*

Figure 5.2

The sock knitted with fibers coated with silver (current conduction) and with fibers having a piezoresistive effect. The central unit (left) is connected to the silver-coated fibers and to a soft battery. *From Perrier A, Vuillerme N, Luboz V, Bucki M, Cannard F, Diot B, Colin D, Rin D, Bourg J-P, Payan Y. Smart Diabetic Socks: embedded device for diabetic foot prevention. IRBM April 2014; 35:72–6.*

therefore highly patient-specific because it depends on the anatomical properties of the patient foot such as the bones curvatures (calcaneus, metatarsal heads, toes) as well as the thicknesses of the soft tissues layers (skin, fat, and muscles). As measuring in vivo and in an embedded way the internal strains of the foot tissues is not possible, we have proposed to quantitatively estimate the internal stresses and strains from the measured external pressures. To achieve this goal, a patient-specific FE model of the foot including soft tissues and bony prominences is specifically built and used to compute the internal strains and stresses (Fig. 5.3).

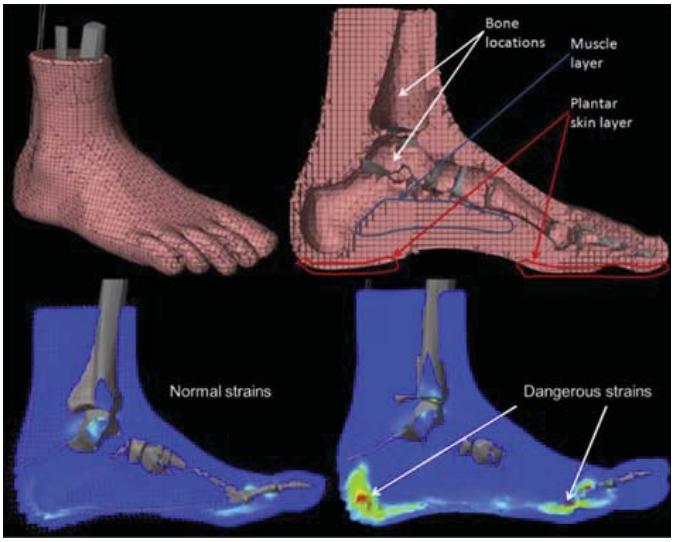

Figure 5.3

Finite element model of the foot: a 3D mesh (top) is used to compute internal strains (bottom). If strain values become too high (as it is illustrated in the lower right panel), an alert is launched. *From Perrier A, Vuillerme N, Luboz V, Bucki M, Cannard F, Diot B, Colin D, Rin D, Bourg J-P, Payan Y. Smart Diabetic Socks: embedded device for diabetic foot prevention. IRBM April 2014; 35:72–6.*

3. A patient-specific foot model

A detailed biomechanical model of the foot has been developed by Perrier et al., 2015. For this, a high-resolution computed tomography (CT) volume acquired on the unloaded right foot of a volunteer was used to segment the 28 bones and reconstruct their 3D shapes. Rigid body contact constraints were implemented in the ArtiSynth framework to model joint interactions. All 33 joint motions were further constrained by 210 ligaments modeled by cables and inserted on the bones using CT images of the subject. Such contacts between bones and ligaments attached to the bones were thus used to guide the foot kinematics. The aponeurosis was modeled using five ligaments linked by transverse structures. Finally, 15 Hills model muscles were positioned according to their anatomical course and can be independently activated. Soft tissues were modeled by an FE mesh comprising three subdomains representing skin, fat, and muscle tissues. The bones were modeled as rigid bodies to accelerate the simulation. The behavior of the bony rigid bodies coupled with FE models of the soft tissue domains was computed using a semiimplicit integration scheme in the ArtiSynth open source framework [7]. To increase the realism from a physiological and a dynamic point of view, the masses of the different structures were estimated using the tables from Ref. [8], which yielded a foot mass of 1.37% of the subject mass. The density and mass of the bones and soft tissues are shown in Table 5.1.

The muscles and part of the ligament insertions were localized within the medical images and the other part of the ligament insertions by resorting to the literature (Fig. 5.4).

The soft tissue FE mesh was generated using a meshing tool provided by the Texisense Company. In this application, modeling domains are defined by the 3D surfaces recovered from medical image segmentation. The meshing algorithm tends to maximize the number of hexahedrons in the generated mesh to avoid the locking effect inherent to linear tetrahedrons in nearly incompressible materials. The final mesh is composed of 23,298 elements and 13,087 nodes. It is composed of four domains: skin, heel fat pad, other fatty tissues, and muscles (see Fig. 5.5). As bones are modeled as rigid bodies, they do not need to be discretized.

To replicate a nonlinear hyperelastic behavior, an isotropic neo-Hookean material is assumed to describe the behavior of the soft tissues. This material behavior is characterized by the strain density energy function given by

$$\Psi = C_{10}(I_1 - 3) + (J - 1)^2 \Big/ D \tag{5.1}$$

Table 5.1: The density and mass of the bones and soft tissues.

	Density (kg/m^3)	Mass (kg)
Bones	1850	0.433
Soft tissues	1200	1.13

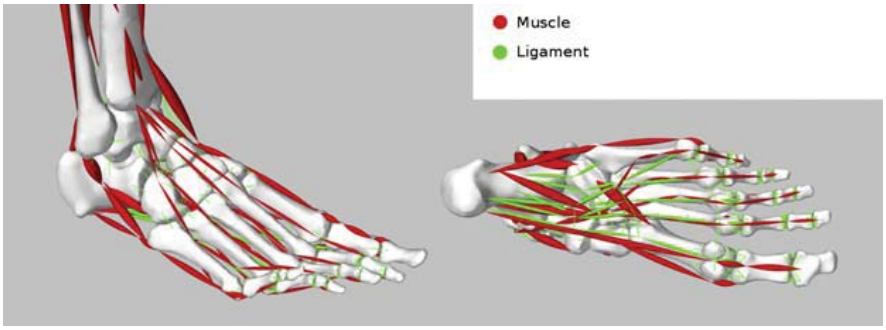

Figure 5.4
The musculoskeletal model with 28 bones, 15 activated muscles (in red), and 210 ligaments (in green). The insertions of those structures have been determined from the MRI scan and from literature.

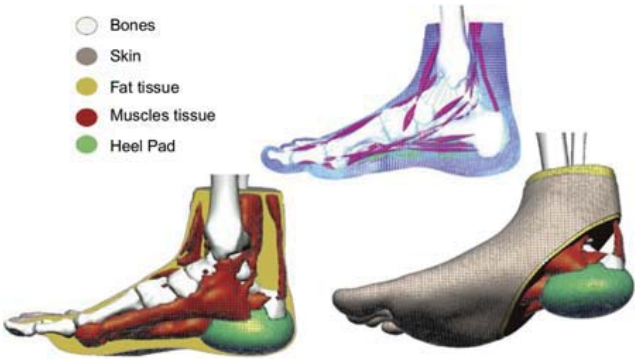

Figure 5.5
The complete biomechanical foot model with bony structures represented as rigid bodies, and soft tissues modeled as a finite element mesh. Soft tissues are divided in four layers: skin (in beige color), heel fat pad (in green), other fatty tissue (in yellow), and muscles (in red). *From Perrier et al., 2017 [3].*

where I_1 is the first invariant of the right Cauchy–Green deformation tensor, C_{10} is a material parameter, J is the determinant of the deformation gradient, and D is a material incompressibility parameter. The material properties of each soft tissue layer (or domain) are shown in Table 5.2 [9]. More details about this model can be found in Perrier et al., 2015, 2017 [20,21].

4. Model order reduction

The technique we used in this work goes by many names as it was employed in different branches of science and engineering among which Karhunen–Loeve (KL) decomposition, POD, or singular value decomposition (SVD) can be mentioned [10–12]., [13,14]. POD was successfully applied to real-time simulation of soft tissue [15–17]. In this work a variation of that method called PODI was used to construct a ROM with a parameter,

which is the muscle activation. Such a model makes it possible to have a fast computation of the field of interest for any value of the parameter [18,19].

4.1 Proper orthogonal decomposition

In this technique we assume that the evolution of a certain field $u(x,t)$is known for example displacements. In practical applications (assuming that some numerical simulations were performed offline, for instance), this field is expressed in a discrete form which is known at the nodes $i$of a spatial mesh at time instancet^m. Thus, we consider that $u(\boldsymbol{x}_i, t^m) \equiv u_i^m$is known. We can also write $\boldsymbol{u}^m$for the vector containing the nodal displacements at time instancet^m. The main idea of KL decomposition is to obtain the most typical or characteristic structure $\phi(\boldsymbol{x})$among these $u^m(\boldsymbol{x})$, $\forall m$. Here ϕ is a scalar field defined at all the nodes of the FE mesh. The characteristic structure is defined in the KL approach as the function that maximizes.

$$\frac{\sum_{m=1}^{M}\left[\sum_{i=1}^{N}\phi(\boldsymbol{x}_i)u^m(\boldsymbol{x}_i)\right]^2}{\sum_{i=1}^{N}(\phi(\boldsymbol{x}_i))^2} \tag{5.2}$$

where N represents the number of nodes of the complete model and M the number of computed time steps. The maximization is equivalent to finding for any direction $\widetilde{\phi}$ the zero of the Gâteaux derivative of the right-hand side in the above equation, which leads to

$$\sum_{m=1}^{M}\left[\left(\sum_{i=1}^{N}\widetilde{\phi}(\boldsymbol{x}_i)u^m(\boldsymbol{x}_i)\right)\left(\sum_{j=1}^{N}\phi(\boldsymbol{x}_j)u^m(\boldsymbol{x}_j)\right)\right] = \alpha\sum_{i=1}^{N}\widetilde{\phi}(\boldsymbol{x}_i)\phi(\boldsymbol{x}_i); \quad \forall\widetilde{\phi} \tag{5.3}$$

which can be rewritten in the form

$$\sum_{i=1}^{N}\left\{\sum_{j=1}^{N}\left[\sum_{m=1}^{M}u^m(\boldsymbol{x}_i)u^m(\boldsymbol{x}_j)\phi(\boldsymbol{x}_j)\right]\widetilde{\phi}(\boldsymbol{x}_i)\right\} = \alpha\sum_{i=1}^{N}\widetilde{\phi}(\boldsymbol{x}_i)\phi(\boldsymbol{x}_i); \ \forall\widetilde{\phi} \tag{5.4}$$

Defining the vector ϕ such that its i-th component is $\phi(\boldsymbol{x}_i)$, Eq. (5.4) takes the following matrix form

$$\widetilde{\boldsymbol{\phi}}^T\boldsymbol{c}\boldsymbol{\phi} = \alpha\boldsymbol{\phi}^T\boldsymbol{\phi}; \forall\widetilde{\boldsymbol{\phi}} \Rightarrow \boldsymbol{c}\boldsymbol{\phi} = \alpha\boldsymbol{\phi} \tag{5.5}$$

Table 5.2: Material properties of the neo-Hookean model for each soft tissue.

	C_{10}	Poisson's ratio
Skin	33.3	0.485
Heel fat pad	16.6	0.499
Other fat tissues	5.0	0.490
Muscles	10.0	0.495

where the two-point correlation matrix is given by

$$c_{ij} = \sum_{m=1}^{M} u^m(\boldsymbol{x}_i) u^m(\boldsymbol{x}_j) \Leftrightarrow \boldsymbol{c} = \sum_{m=1}^{M} \boldsymbol{u}^m (\boldsymbol{u}^m)^T \tag{5.6}$$

which is symmetric and positive definite. If we define the matrix $\boldsymbol{Q}$ containing the discrete field history:

$$\boldsymbol{Q} = \begin{pmatrix} u_1^1 & u_1^2 & \cdots & u_1^M \\ u_2^1 & u_2^2 & \cdots & u_2^M \\ \vdots & \vdots & \ddots & \vdots \\ u_N^1 & u_N^2 & \cdots & u_N^M \end{pmatrix} \tag{5.7}$$

then it is easy to verify that the matrix c in Eq. (5.5) results

$$c = \boldsymbol{Q}\boldsymbol{Q}^T \tag{5.8}$$

If some simulations were carried out, we can determine $\boldsymbol{u_i^m}$, $\forall i \in [1, \cdots, N]$and $\forall m \in [1, \cdots, M]$, and from these solutions the r modes related to the r-highest eigenvalues that are expected to contain the most important information about the problem solution. For this purpose we solve the eigenvalue problem defined by Eq. (5.5) retaining the modes corresponding to the eigenvalues that sum up to 99% of the variance. In practice, r is much lower than N, and this constitutes the main advantage of the technique. Thus, we can try to use these r eigenmodes $\phi_k$for approximating the solution of a problem *slightly* different to the one that has served to define u_j^m. For this purpose we define the matrix $\boldsymbol{A} = [\phi_1 \cdots \phi_r]$, which is an orthonormal basis

$$\boldsymbol{A} = \begin{pmatrix} \phi_1(\boldsymbol{x}_1) & \phi_2(\boldsymbol{x}_1) & \cdots & \phi_r(\boldsymbol{x}_1) \\ \phi_1(\boldsymbol{x}_2) & \phi_2(\boldsymbol{x}_2) & \cdots & \phi_r(\boldsymbol{x}_2) \\ \vdots & \vdots & \ddots & \vdots \\ \phi_1(\boldsymbol{x}_N) & \phi_2(\boldsymbol{x}_N) & \cdots & \phi_r(\boldsymbol{x}_N) \end{pmatrix} \tag{5.9}$$

Now, assuming that the displacement vector contains the nodal degrees of freedom, it can be expressed as

$$\boldsymbol{u}^m = \sum_{i=1}^{r} \boldsymbol{\zeta}_i^m \phi_i = \boldsymbol{A}\,\boldsymbol{\zeta}^m \tag{5.10}$$

in which $\boldsymbol{\zeta}^m$ are the coordinates with respect to the POD basis. They are sometimes referred to as the reduced coordinates. It is worth reiterating that as r is much smaller than N, the displacement vector could be expressed with a few reduced coordinates.

4.2 Proper orthogonal decomposition with interpolation

In the previous section, POD procedure was explained considering a time-varying field, although that procedure can be applied in parameter space for example computing displacements by varying a parameter [18,19]. In this work, muscle activations were used as parameters and the displacement field was obtained for a range of physiological values. The procedure for fast prediction of the displacement field u for any value of the parameter γ can be summarized as

1. Perform simulations for each parameter value $\gamma_i$to obtain snapshots $\boldsymbol{u}^{\gamma i}$.
2. Apply POD technique to obtain the matrix $\boldsymbol{A}$ in Eq. (5.9), which is the orthonormal basis.
3. Compute the reduced coordinates for each snapshot using the inner product as

$$\zeta_j^{\gamma_i} = \left(\boldsymbol{u}^{\gamma_i}, \phi_j\right) \tag{5.11}$$

4. The reduced coordinates for intermediate values of γ that were not included in constructing POD basis are calculated by cubic spline interpolation of $\boldsymbol{\zeta}^{\gamma i}$, which is the vector containing the reduced coordinates corresponding to the parameter value γ_i. Now, the displacement field for this parameter value can be calculated using Eq. (5.4) as

$$\boldsymbol{u}^{\gamma} = \sum_{i=1}^{r} \zeta_i^r \phi_i = \boldsymbol{A}\boldsymbol{\zeta}^{\gamma}$$

Remark 1: Often, one is interested in finding rather an approximating affine subspace than a linear subspace. Hence the snapshots are centered by subtracting its average $\overline{\boldsymbol{u}}$ and collect the centered vectors as columns of the matrix $\boldsymbol{Q}$.

Remark 2: POD modes can also be computed by SVD of $\boldsymbol{Q}$ $\boldsymbol{Q}(\boldsymbol{U}\sum \boldsymbol{V}^T)$. In that case the POD modes are the columns of $\boldsymbol{U}$.

Remark 3: In many applications N is very large and calculation of the POD modes would require solving a large eigenvalue problem, which is not feasible. In such cases the modes can be computed by the method of snapshots proposed by Ref. [11].

5. Results and discussion

As a preliminary result, to investigate the ability of the model order reduction technique to run our foot model in an interactive way, one example is considered. In this example, the tibialis anterior muscle was activated and the displacement field was achieved using the ArtiSynth program. Afterward, the POD was applied to these solutions to construct a ROM with the muscle activation as a parameter. The force exerted by the tibialis anterior

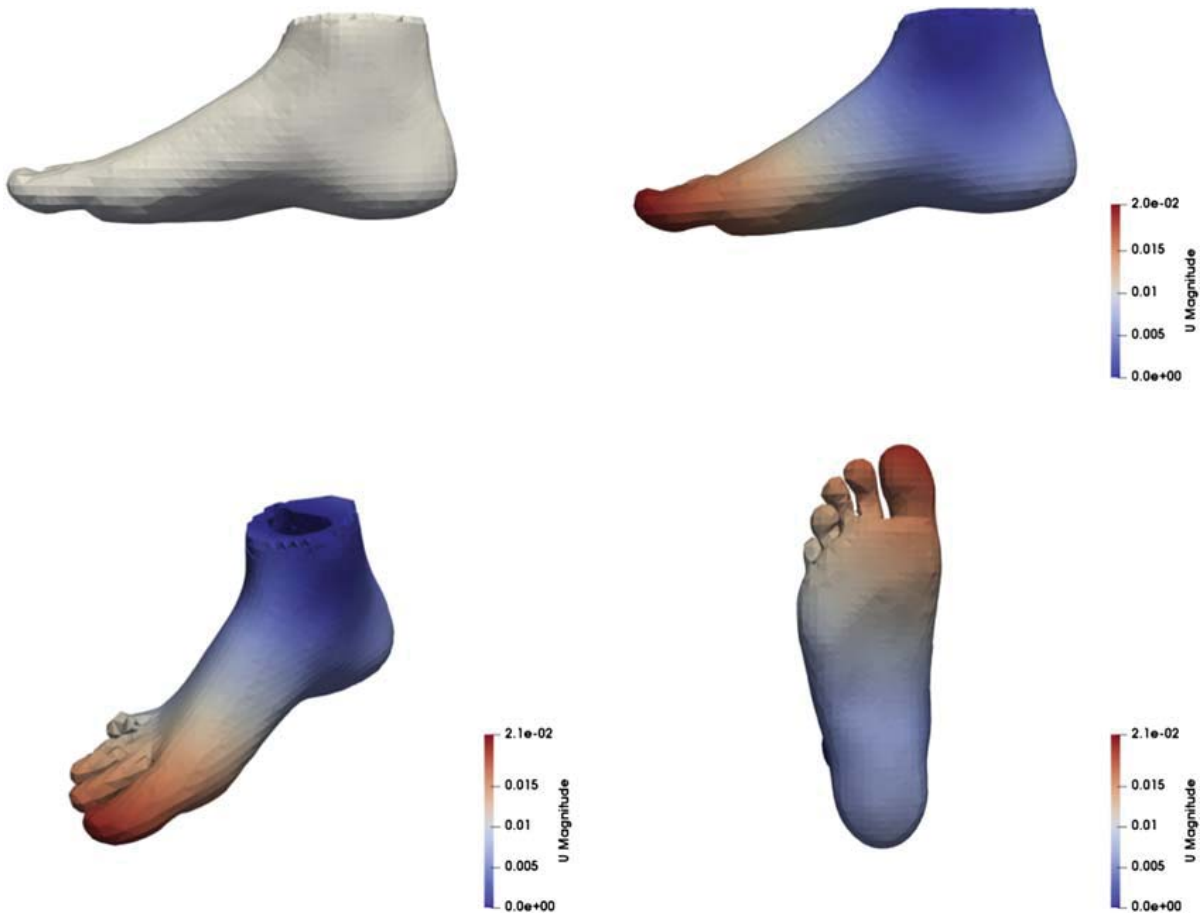

Figure 5.6
The nodal displacement magnitude for the first eigenmode.

muscle is increased from 0% to 70% of its maximum value and the displacement field of the FE model is computed by ArtiSynth and saved at each interval along with the muscle activation value (with a total of 200 simulated results). If we consider the muscle activation as a parameter, we can use PODI technique to have a fast prediction of the displacement field for any parameter value between 0% and 70%. We used 101 snapshots to construct the ROM and 99 snapshots to evaluate the ROM for intermediate values of muscle activation. The nodal displacement magnitudes for the first three eigenmodes are shown in Figs. 5.6–5.8.

The displacement field due to the tibialis anterior muscle 70% activation and computed by ArtiSynth from one side and by the ROM from the other side are depicted in Figs. 5.9 and 5.10, respectively.

As it can be seen, the ROM solution has a good agreement with the ArtiSynth solution, which is considered as the reference solution. The evolution of the relative error norm with muscle activation is plotted in Fig. 5.11 and the error in displacement

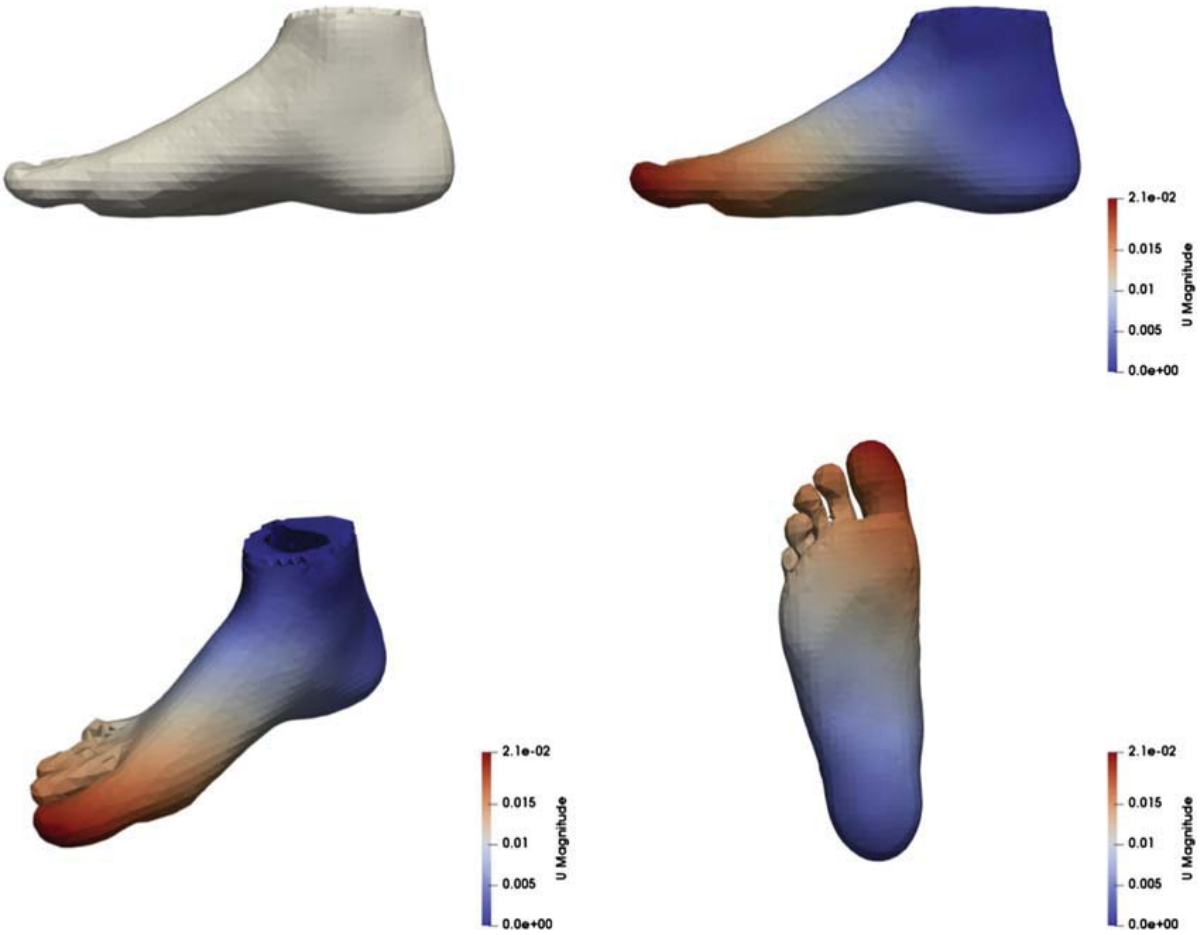

Figure 5.7
The nodal displacement magnitude for the second eigenmode.

$\|\boldsymbol{U}_{PODI} - \boldsymbol{U}_{Art}\|$was computed in the whole foot volume to determine the zones with less accurate results, which are around the ball of the foot and the tip of the big toe (Fig. 5.12).

The nodes around the big toe have large displacements and the node with maximum displacement was picked. The evolution of this value with the muscle activation calculated using the ArtiSynth program and the ROM is plotted in Fig. 5.13.

The computation time using ArtiSynth was about 12 h on a PC running Linux Mint with Intel Xeon CPU E5-1607 at 3 GHz; only four cores were used. Once the ROM is constructed, the displacement field generated by any activation of the tibialis anterior muscle requires 0.1 s to be computed. Despite such short computation time, the results of the ROM show good accuracy in comparison to the ArtiSynth solution because the maximum relative error norm was 3.8%, which seems acceptable in clinical routine. This technique could equally be extended to use an online version of the foot model by applying pressure values measured by the smart sock.

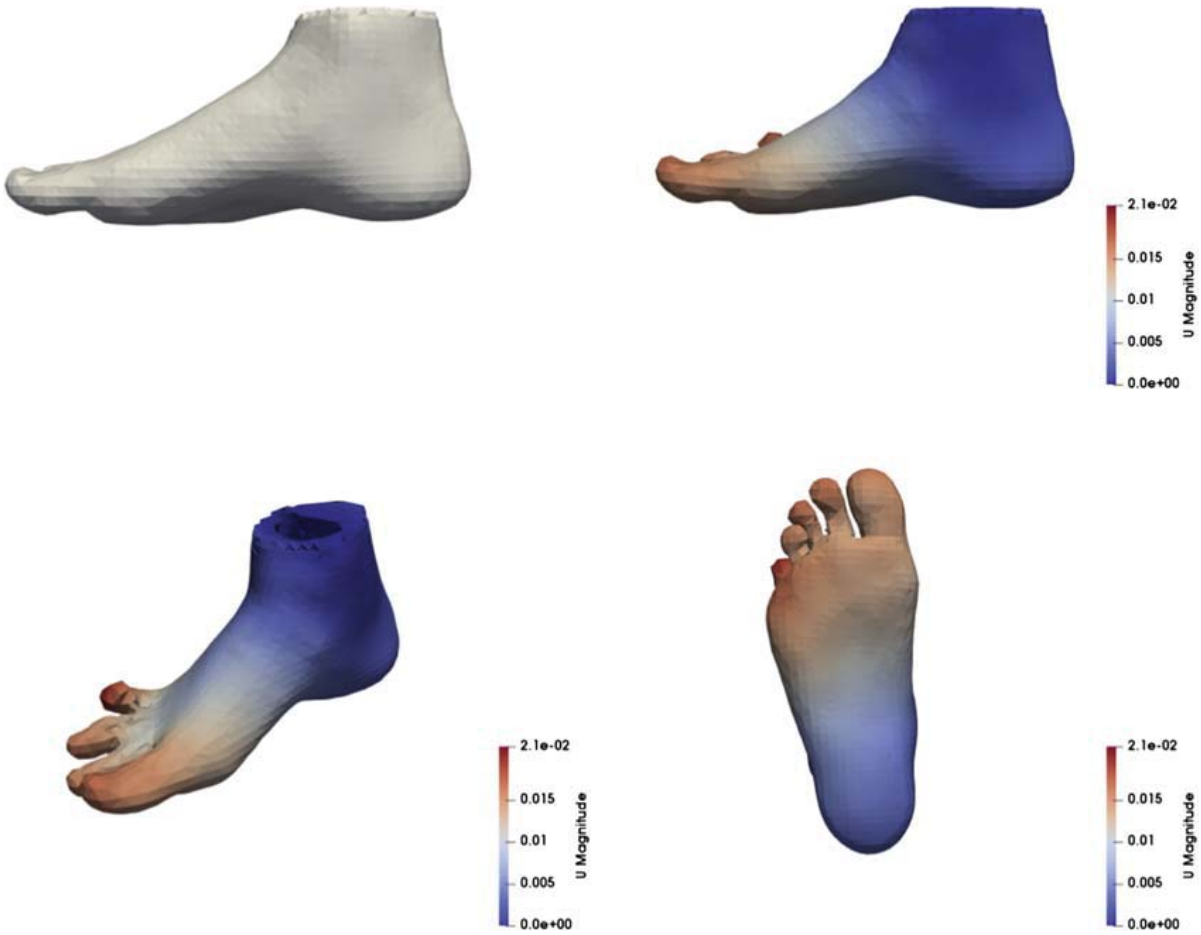

Figure 5.8
The nodal displacement magnitude for the third eigenmode.

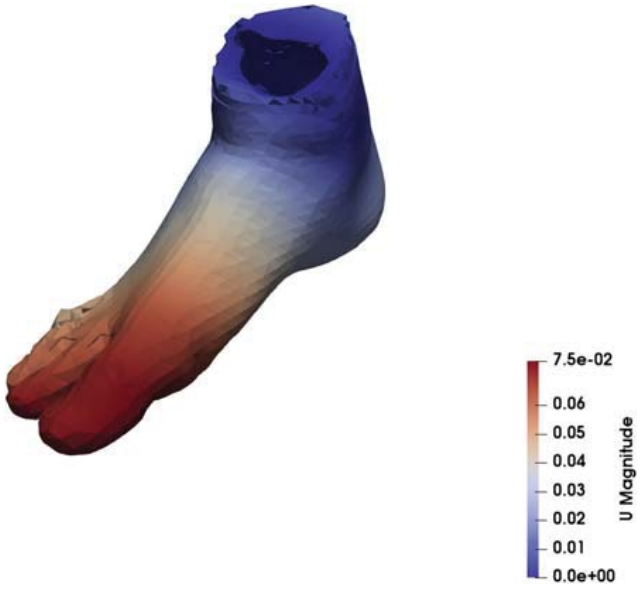

Figure 5.9
The displacement field computed by the ArtiSynth program.

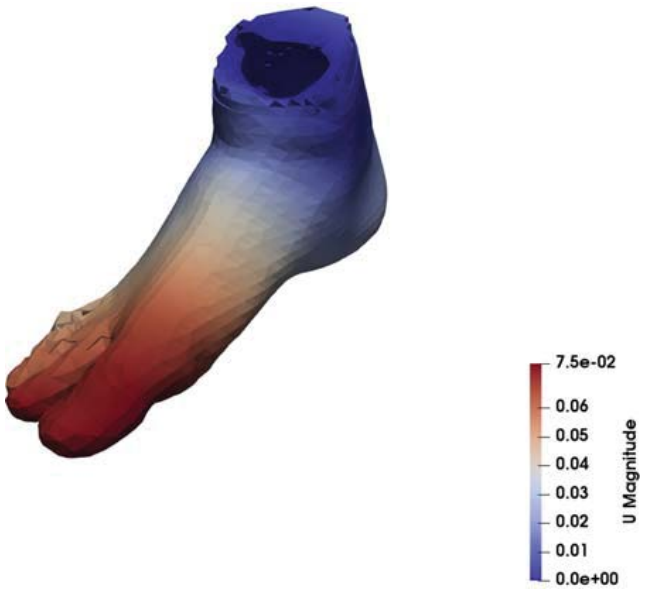

Figure 5.10
The displacement field computed by the reduced order model.

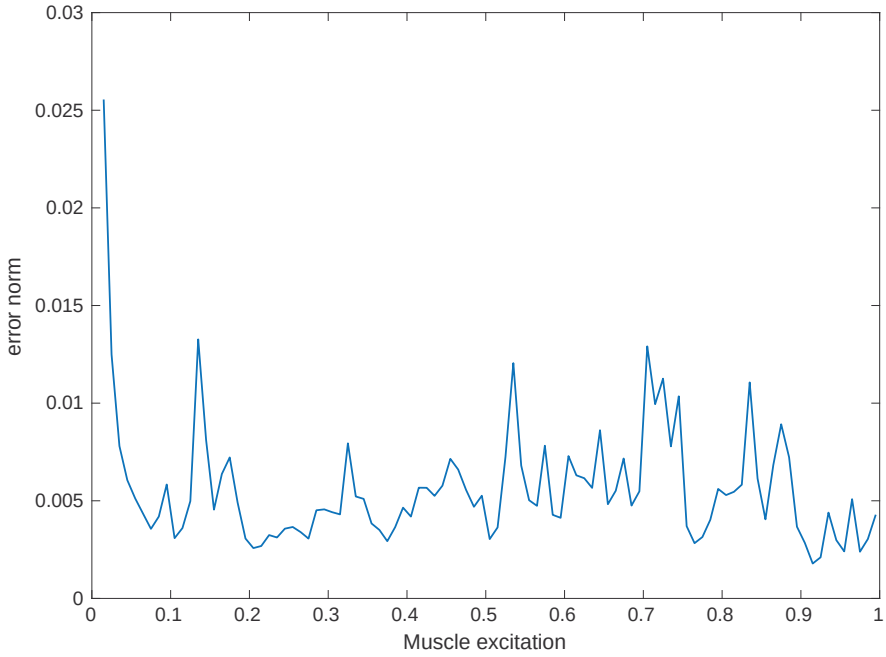

Figure 5.11
The relative error norm evolution with muscle activation.

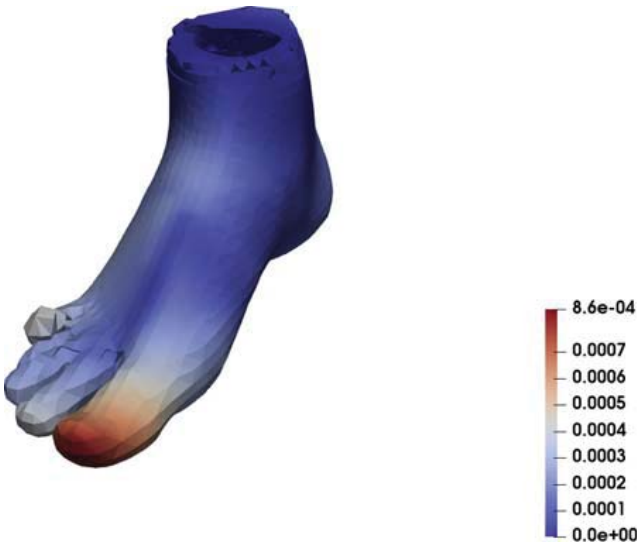

Figure 5.12
The error in displacement for the whole foot.

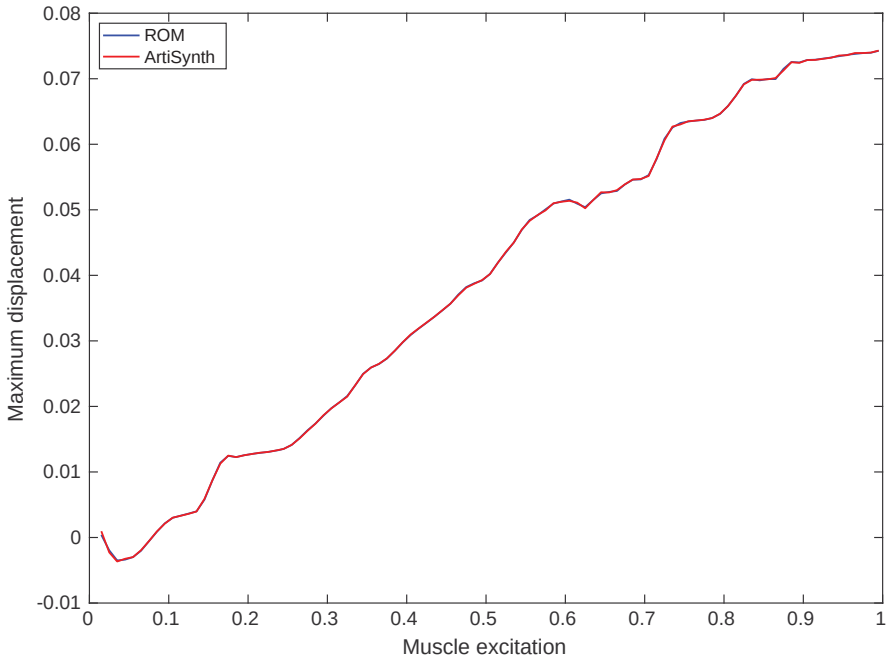

Figure 5.13
The maximum displacement evolution with muscle activation. *ROM*, reduced order model.

Acknowledgments

This work was funded by the *Fondation pour la Recherche Médicale* under the project FRM DIC20161236448.

References

[1] Shaw JE, Boulton AJM. The pathogenesis of diabetic foot problems: an overview. Diabetes 1997;46(Suppl. 2):S58−61. https://doi.org/10.2337/diab.46.2.S58. ISSN 0012-1797.
[2] Boulton AJM, Vileikyte L, Ragnarson-Tennvall G, Jan A. The global burden of diabetic foot disease. Lancet 2005;366:1719−24.
[3] Perrier A, Vuillerme N, Luboz V, Bucki M, Cannard F, Diot B, Colin D, Rin D, Bourg J-P, Payan Y. Smart Diabetic Socks: embedded device for diabetic foot prevention. IRBM April 2014;35:72−6.
[4] Atlas E, Yizhar Z, Khamis S, Slomka N, Shlomo H, Amit G. Utilization of the foot load monitor for evaluating deep plantar tissue stresses in patients with diabetes: proof-of-concept studies. Gait Posture 2009;29(3):377−82. ISSN 0966-6362.
[5] Linder-Ganz E, Shabshin N, Itzchak Y, Yizhar Z, Siev-Ner I, Gefen A. Strains and stresses in sub-dermal tissues of the buttocks are greater in paraplegics than in healthy during sitting. J Biomech 2008;41(3):567−80.
[6] Loerakker S, Manders E, Strijkers GJ, Nicolay K, Baaijens FPT, Bader DL, Oomens CWJ. The effects of deformation, ischemia, and reperfusion on the development of muscle damage during prolonged loading. J Appl Physiol 2011;111(4):1168−77. https://doi.org/10.1152/japplphysiol.00389.2011. PMID: 21757578.
[7] Lloyd JE. Ian Stavness, and Sidney Fels. Artisynth: a fast interactive biomechanical modeling toolkit combining multibody and finite element simulation. In: Payan Y, editor. Soft tissue biomechanical modeling for computer assisted surgery. Springer Berlin Heidelberg; 2012. p. 355−94.
[8] de Leva P. Adjustments to zatsiorsky-seluyanovs segment inertia parameters. J Biomech 1996;29(9):1223−30.
[9] Luboz V, Perrier A, Bucki M, Diot B, Cannard F, Vuillerme N, Payan Y. Influence of the calcaneus shape on the risk of posterior heel ulcer using 3d patient-specific biomechanical modeling. Ann Biomed Eng February 2015;43(2):325−35. https://doi.org/10.1007/s10439-014-1182-6. ISSN 1573-9686.
[10] Karhunen K. Uber lineare methoden in der wahrscheinlichkeitsrechnung. Ann Acad Sci Fennicae, Ser Al Math Phys 1946;37.
[11] Sirovich L. Turbulence and the dynamics of coherent structures. i - iii. Q Appl Math 1987;45(3):561−1590.
[12] P. Krysl, S. Lall, and J. E. Marsden. Dimensional model reduction in non-linear finite element dynamics of solids and structures. Int J Numer Methods Eng 51(4):479−504. https://doi.org/10.1002/nme.167.
[13] Liang YC, Lee HP, Lim SP, Lin WZ, Lee KH, Wu CG. Proper orthogonal decomposition and its applications-part I: Theory. J Sound Vib 2002;252(3):527−44. ISSN 0022-460X, https://doi.org/10.1006/jsvi.2001.4041.
[14] Pinnau R. Model reduction via proper orthogonal decomposition. In: Model order reduction: theory, research aspects and applications, vol. 13. Springer-Verlag Berlin Heidelberg; 2008. p. 95−109.
[15] Niroomandi S, Alfaro I, Cueto E, Chinesta F. Real-time deformable models of non-linear tissues by model reduction techniques. Comput Methods Progr Biomed 2008;91(3):223−31. https://doi.org/10.1016/j.cmpb.2008.04.008. ISSN 01692607.
[16] Niroomandi S, Alfaro I, Cueto E, Chinesta F. Accounting for large deformations in real-time simulations of soft tissues based on reduced-order models. Comput Meth Prog Bio 2010. https://doi.org/10.1016/j.cmpb.2010.06.012. ISSN 0169-2607.
[17] Cueto E, Chinesta F. Real time simulation for computational surgery: a review. Adv Model Simul Eng Sci April 2014;1(1):11. https://doi.org/10.1186/2213-7467-1-11. ISSN 2213-7467.

[18] Ly HV, Tran HT. Modeling and control of physical processes using proper orthogonal decomposition. Math Comput Model 2001;33(1):223−36. ISSN 0895-7177, https://doi.org/10.1016/S0895-7177(00)00240-5. Computation and control VI proceedings of the sixth Bozeman conference.
[19] Epureanu BI, Dowell EH, Hall KC. A parametric analysis of reduced order models of potential flows in turbomachinery using proper orthogonal decomposition. In: ASME TURBO EXPO; 2001. 2001.
[20] Perrier A, Bucki M, Vincent L, Vuillerme N, Payan Y. 3D musculoskeletal finite element analysis of the foot kinematics under muscle activation with and without ankle arthrodesis. Comput Methods Biomech Biomed Eng 2015;0(0):1−2. https://doi.org/10.1080/10255842.2015.1069605. PMID: 26273957.
[21] Antoine P, Vincent L, Bucki M, Cannard F, Vuillerme N, Payan Y. Biomechanical modeling of the foot. In: Biomechanics of living organs: hyperelastic constitutive laws for finite element modeling. Academic Press; 2017. p. 545−63.
[22] Gefen A. Plantar soft tissue loading under the medial metatarsals in the standing diabetic foot. Med Eng Phys 2003;25(6):491−9. ISSN 1350-4533.